OXFORD

Cerebral Cortex, May 2020;30: 2972–2985

doi: 10.1093/cercor/bhz288
Advance Access Publication Date: 10 December 2019
Original Article

ORIGINAL ARTICLE

Enhancing Plasticity Mechanisms in the Mouse Motor Cortex by Anodal Transcranial Direct-Current Stimulation: The Contribution of Nitric Oxide Signaling

Saviana Antonella Barbati[1], Sara Cocco[1], Valentina Longo[1], Matteo Spinelli[1], Katia Gironi[1], Andrea Mattera[1], Fabiola Paciello[1], Claudia Colussi[1,2], Maria Vittoria Podda[1,3] and Claudio Grassi[1,3]

[1]Istituto di Fisiologia Umana, Università Cattolica del Sacro Cuore, Roma 00168, Italy, [2]Istituto di Analisi dei Sistemi ed Informatica "Antonio Ruberti" (IASI) - CNR, Rome 00185, Italy, and [3]Fondazione Policlinico Universitario A. Gemelli IRCCS, Roma 00168, Italy

Address correspondence to: Maria Vittoria Podda, Istituto di Fisiologia Umana, Università Cattolica del Sacro Cuore, Largo F. Vito, 1, 00168 Roma, Italy. Email: mariavittoria.podda@unicatt.it.

S.A.B. and S.C. contributed equally to this work.

Abstract

Consistent body of evidence shows that transcranial direct-current stimulation (tDCS) over the primary motor cortex (M1) facilitates motor learning and promotes recovery after stroke. However, the knowledge of molecular mechanisms behind tDCS effects needs to be deepened for a more rational use of this technique in clinical settings. Here we characterized the effects of anodal tDCS of M1, focusing on its impact on glutamatergic synaptic transmission and plasticity. Mice subjected to tDCS displayed increased long-term potentiation (LTP) and enhanced basal synaptic transmission at layer II/III horizontal connections. They performed better than sham-stimulated mice in the single-pellet reaching task and exhibited increased forelimb strength. Dendritic spine density of layer II/III pyramidal neurons was also increased by tDCS. At molecular level, tDCS enhanced: 1) BDNF expression, 2) phosphorylation of CREB, CaMKII, and GluA1, and 3) S-nitrosylation of GluA1 and HDAC2. Blockade of nitric oxide synthesis by L-NAME prevented the tDCS-induced enhancement of GluA1 phosphorylation at Ser831 and BDNF levels, as well as of miniature excitatory postsynaptic current (mEPSC) frequency, LTP and reaching performance. Collectively, these findings demonstrate that anodal tDCS engages plasticity mechanisms in the M1 and highlight a role for nitric oxide (NO) as a novel mediator of tDCS effects.

Key words: AMPA receptor, BDNF, long-term potentiation, nitrosylation, personalized medicine

Introduction

TDCS has recently gained much attention due to its effectiveness in modulating cortical functions (Brasil-Neto 2012; Lefaucheur 2016; Buch et al. 2017). One of the most substantiated and promising applications is the use of tDCS in targeting M1 to modulate motor skill learning and memory in physiological conditions and to promote motor recovery after stroke (Reis et al. 2008, 2009; Zimerman et al. 2012; Buch et al. 2017; Lefebvre and Liew 2017).

Early evidence showed that anodal tDCS over M1 increases motor cortical excitability (Nitsche and Paulus 2000; Cambiaghi et al. 2010). The long-lasting effects of tDCS on neuronal excitability and motor behavior suggested the possible engagement of plasticity-like mechanisms (Nitsche et al. 2003; Cheeran et al. 2008; Cirillo et al. 2017). Indeed, Fritsch and colleagues (Fritsch et al. 2010) demonstrated that anodal DCS applied to M1 slices, concomitantly with synaptic activation, induced NMDA receptor (NMDAR)-dependent LTP, a well-established form of activity-dependent long-term changes in synaptic efficacy (Malenka and Bear 2004). Of relevance, the involvement of NMDAR in mediating tDCS effect on plasticity is also supported by human studies (Nitsche et al. 2003, 2004). Since these first observations, numerous studies have demonstrated the effect of tDCS on the rodent hippocampus—the best characterized and most widely used model to study LTP and LTP-dependent behavioral correlates (i.e., learning and memory). These studies provided solid and converging evidence that anodal tDCS enhances LTP at CA3-CA1 synapses (Ranieri et al. 2012; Rohan et al. 2015; Podda et al. 2016; Kronberg et al. 2017) and affects molecular determinants of synaptic plasticity, including immediate early genes, such as *c-fos* and activity regulated cytoskeleton-associated protein (Arc) (Ranieri et al. 2012; Kim et al. 2017), brain-derived neurotrophic factor (BDNF), phosphorylation of CREB at Ser133 (pCREB^{Ser133}) (Podda et al. 2016) and of AMPA receptor GluA1 subunit at Ser831 (pGluA1^{Ser831}) (Stafford et al. 2018). Building on this evidence and considering the well-documented changes in M1 glutamatergic transmission and plasticity in motor skill learning and memory, we investigated the effects of anodal tDCS on M1 focusing on LTP and glutamatergic synaptic transmission at layer II-III horizontal connections, the main site of plasticity associated with motor skill learning (Hess and Donoghue 1994, 1996; Rioult-Pedotti et al. 1998; Kida et al. 2016, 2018). Here we report that enhanced forelimb strength and skilled performance in mice subjected to anodal tDCS are associated with increased synaptic transmission and plasticity at M1 layer II/III horizontal connections, increased spine density in apical and basal arborizations of layer II/III pyramidal neurons and enhanced expression of BDNF and phosphorylation of CREB, Ca^{2+}/calmodulin-dependent kinase II (CaMKII) and GluA1. Moreover, tDCS-induced effects were prevented by inhibition of NO synthesis.

Materials and Methods

Animals

Male C57BL/6 mice (30–45-day-old) were used. All animal procedures were approved by the Ethics Committee of the Catholic University and were fully compliant with Italian Ministry of Health guidelines (Legislative Decree No. 26/2014) and European Union (Directive No. 2010/63/UE) legislation on animal research. The methods were carried out in strict accordance with the approved guidelines. The animals were housed under a 12-h light–dark cycle at a controlled temperature (22–23°C) and constant humidity (60–75%). All efforts were made to limit the number of animals used and to minimize their suffering. Mice were randomly assigned to the following experimental groups: 1) control mice, which underwent surgical procedures for electrode implantation and were subjected to sham stimulation and 2) tDCS mice, which were subjected to anodal tDCS. Different groups of mice were used for each experimental test.

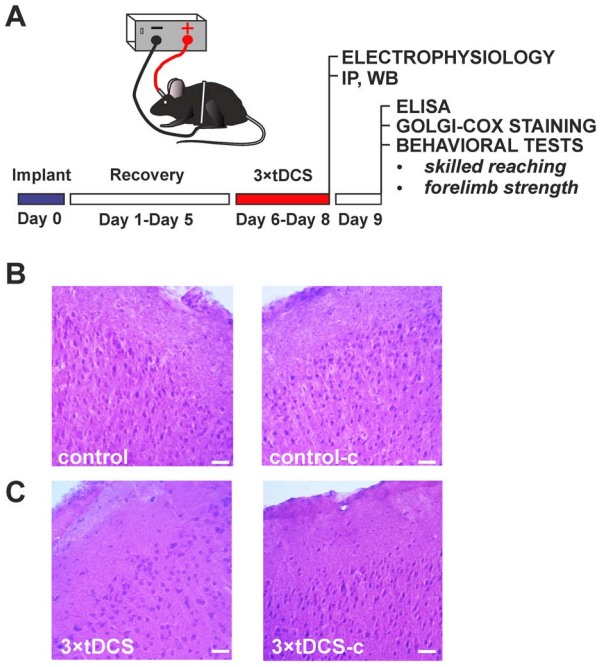

Figure 1. Experimental design and hematoxylin–eosin staining of M1. *A*: Adult male C57BL/6 mice were implanted with an epicranial electrode and allowed to recover from surgery before undergoing sham stimulation or 3 × tDCS protocol consisting of a single daily tDCS session (250 µA for 20 min) for 3 consecutive days. Different groups of animals were used for each experimental protocol at different time points. Electrophysiology (field and patch-clamp recordings); behavioral tests were used to assess forelimb skilled reaching and strength. *B,C*: Representative M1 sections stained with hematoxylin–eosin obtained from control mice (*B*) and 3 × tDCS mice (*C*); M1 hemispheres contralateral to the epicranial cannula (*c*) are shown in the right hand panels. No significant differences or tissue damage were observed across sections. Scale bar = 20 µm.

All experimental procedures were performed according to previously published protocols with minor modifications. Detailed description of methodology is provided in Supplementary Materials and methods.

Electrode Implantation and tDCS Protocol

TDCS over M1 was delivered using a unilateral epicranial electrode arrangement (Podda et al. 2016; Paciello et al. 2018). The active electrode consisted of a tubular plastic cannula (internal diameter 3.0 mm) filled with saline solution (0.9% NaCl) just prior to stimulation; the counter electrode was a conventional rubber-plate electrode surrounded by a wet sponge (5.2 cm^2) positioned over the ventral thorax (Fig. 1A).

For electrode implantation, animals were anesthetized by intraperitoneal injection of a cocktail containing ketamine (87.5 mg/kg) and xylazine (12.5 mg/kg). Duringsurgery, temperature was maintained at 37°C. The scalp and underlying tissues were removed and the electrode was implanted using a carboxylate cement (3 M ESPE, Durelon, 3 M Deutschland GmbH, Germany). The center of the active electrode was positioned on the skull over the M1 (+1.4 mm antero–posterior and 2 mm lateral to the bregma) (Franklin and Paxinos 1997). After surgery, all animals were allowed to recover for 3–5 days before undergoing tDCS. During this period, as well as during the electrical stimulations, mice were placed in individual cages.

TDCS was applied to awake mice using a battery-driven, constant current stimulator (BrainSTIM, EMS, Italy). The current

intensity was ramped for 10 s instead of switching it on and off directly to avoid a stimulation break effect.

A repeated tDCS protocol was used, consisting of 3 single stimulation sessions (at a current intensity of 250 μA for 20 min, current density of 35.4 A/m^2) on 3 consecutive days, once per day (hereinafter referred to as 3 × tDCS).

According to clinical and brain slice convention (Jackson et al. 2016; Rahman et al. 2017), "anodal" tDCS was applied, corresponding to a positive electric field (positive electrode on the motor cortex).

On each day, tDCS intervention was performed at approximately the same time of day (around 10 a.m.). No abnormal behaviors were observed related to the stimulation and no morphological alterations were found in brain tissues of mice subjected to tDCS (Fig. 1B,C). Control animals underwent the same protocol as the "real" stimulation condition, but no current was delivered (sham stimulation).

Histological Processing

Histological evaluation was carried out to detect possible current-induced neurotrauma (e.g., oedema, necrosis, haematoma, and cellular alterations). At the end of the stimulation session, animals were anesthetized by intraperitoneal injection of a cocktail containing ketamine (87.5 mg/kg) and xylazine (12.5 mg/kg), and perfused transcardially with saline followed by a fixative containing 4% paraformaldehyde in 0.1 M phosphate-buffered saline (PBS). After postfixation, brains were removed from the skulls and stored at 4°C in a high sucrose solution (30% sucrose in 0.1 M PBS) for 2 days. A cryostat (SLEE:MEV) was used to collect serial coronal 30-μm thick sections containing the M1. All sections were further processed for hematoxylin–eosin staining (Podda et al. 2016). Images were acquired with a Zeiss AxioPhot Microscope.

To evaluate the effect of 3 × tDCS on spine density in the M1, Golgi-Cox staining was performed 24 h after the last stimulation session, according to previously published protocols (Paciello et al. 2018). The stained sections were analyzed using confocal laser scanning system (Nikon Ti-E, Confocal Head A1 MP, Tokyo, Japan) with a ×63 oil-immersion objective lens. Cortical pyramidal neurons of layer II/III were identified by the presence of a basal dendritic tree, distinct single apical dendrite and dendritic spines. A researcher who was unaware of the identity of the specimens performed spine density evaluation in each neuron analyzed. Apical and basal dendritic trees were separately examined and spine density was calculated along a 25 μm length of the apical and basal dendrites. Representative images were acquired by using Olympus BX63 microscope with a ×60 oil-immersion objective lens.

Electrophysiology

Whole-cell and field recordings were performed on M1 coronal slices (300- and 400-μm-thick, respectively) according to published protocols (Podda et al. 2008, 2016; Kida et al. 2016). M1 was identified based on its position relative to the lateral ventricle, the anterior commissure, striatum and midline. Slices containing the stimulated M1 were used for subsequent analyses. All recordings were made using a MultiClamp 700B amplifier (Molecular Devices). Data acquisition and stimulation protocols were performed with the Digidata 1440A Series interface and pClamp 10 software (Molecular Devices). Data were filtered at 1 kHz, digitized at 10 kHz, and analyzed both online and offline. Synaptic responses were elicited by electrical stimulation (80 μs duration) of M1 layer II/III using a concentric bipolar tungsten electrode (FHC Inc., Bowdoin, ME, USA) connected to a stimulator (Fig. 3A). Field recordings were made using glass pipettes filled with aCSF (tip resistance 2–5 MΩ) and placed in layer II/III, ~200 μm lateral to the stimulating electrode. The stimulation intensity that produced 50% of the maximal response was used for the test pulses and LTP induction. For LTP recordings, stable baseline responses to test stimulations (0.05 Hz for 10 min) were recorded. This was followed by theta-burst stimulation (TBS), delivered at layer II/III horizontal connections during a transient reduction of GABAA-receptor-dependent synaptic inhibition by 1.5-min bath application of 10 μM bicuculline methiodide (Supplementary Fig. 1A,B). LTP induction protocol consisted of five TBS delivered every 10 s (0.1 Hz). Each TBS consisted of 10 bursts (1 burst = 5 pulses at 100 Hz) delivered at 5 Hz. For the analysis of LTP, the peak amplitude of field excitatory postsynaptic potentials (fEPSPs) was chosen, since the slope was frequently contaminated by the appearance of a first component insensitive to the AMPA receptor antagonist NBQX, likely due to antidromic activity in M1 (Castro-Alamancos et al. 1995; Fritsch et al. 2010) (Supplementary Fig. 1C,D). The fEPSP amplitude was measured from baseline to peak. Before the LTP induction protocol, to check for a possible effect of tDCS on basal synaptic transmission, input/output (I/O) curves were obtained by recording fEPSPs induced by presynaptic stimulation, at intensities ranging from 0 to 30 V (in 5 V-steps). Moreover, using the same protocol described above, LTP at vertical connections-layer II/III pyramidal neuron synapses was also evaluated by placing the stimulation electrode in layer V and the recording electrode in layer II/III.

Whole-cell voltage-clamp recordings were performed from visually identified layer II/III pyramidal neurons to measure paired-pulse ratio (PPR), AMPA/NMDA ratio, miniature excitatory and inhibitory postsynaptic currents (mEPSCs and mIPSCs, respectively). PPR was measured at 20 ms (PPR20) and 50 ms (PPR50) interpulse intervals and was expressed as the ratio of the second response with respect to the first response. AMPA/NMDA ratio was expressed as the ratio between the peak amplitude of the EPSCs recorded at −60 mV and the peak amplitude of the EPSCs recorded at +40 mV in the presence of NBQX (10 μM). For PPR, AMPA/NMDA ratio and mEPSCs recordings, picrotoxin (40 μM) was applied to block GABAergic ionotropic transmission; tetrodotoxin (TTX, 1 μM) was also added for mEPSC recordings. mIPSCs were recorded according to published protocol (Leggio et al., 2019). These recordings were performed in the presence of TTX (1 μM) and NBQX (20 μM) by using electrodes filled with internal solution containing (in mM): 135 CsCl, 10 EGTA, 10 HEPES, 5 ATP-Mg, and 5 QX-314 (pH: 7.30; 290–295 mOsm/l). For the other patch-clamp recordings, the electrode was filled with internal solution containing (in mM): 135 $CsMeSO_3$, 8 NaCl, 10 HEPES, 0.25 EGTA, 2 Mg_2ATP, 0.3 Na_3GTP, 0.1 spermine, 7 phosphocreatine, and 5 QX-314 (pH: 7.25–7.30; 294–298 mOsm/l).

The access resistance and membrane capacity was monitored before and at the end of the experiments; recordings were considered stable when the series and input resistances, resting membrane potential, and stimulus artifact duration did not change (>20%).

Western Immunoblot

Total proteins were extracted from the stimulated motor cortex of control and 3 × tDCS-mice sacrificed 2 h after stimulation,

using ice-cold RIPA buffer as previously reported (Podda et al. 2016). Protein lysates (40 µg) were loaded onto 10% Tris-glycine polyacrylamide gels for electrophoretic separation. Precision Plus Protein Dual Color Standards (Bio-Rad) were used as molecular mass standards. The following primary antibodies were used: pCREB^{Ser133}, CREB, pCaMKII^{Thr286}, CaMKII, pGluA1^{Ser831}, GluA1, and tubulin (Supplementary Table 1). After three 10-min washes in Tris-buffered saline, 0.1% Tween 20 (TBST), membranes were incubated for 1 h at RT with HRP-conjugated secondary antibodies (Supplementary Table 1). The membranes were again washed in TBST, and the bands were visualized with an enhanced chemiluminescence detection kit (GE Healthcare, UK). Protein expression was evaluated and documented by using UVItec Cambridge Alliance.

Protein Nitrosylation Analysis

Immunoprecipitations (IPs) were performed using 3 µg of antibody for 250 µg of total protein in IP buffer (TrisHCl 50 mM pH 7.5, NaCl 300 mM, NP-40 1%, EDTA 5 mM, plus protease inhibitor mix) with the Ademtech's *Bio-Adembeads* paramagnetic bead system. A negative control was performed with the same amount of protein extract sample, immunoprecipitated with the corresponding purified IgG (Santa Cruz). After IP with anti-GluA1 antibody, samples were analyzed by Western blot and the presence of nitrosylation detected by anti-nitroso-cysteine antibody (Supplementary Table 1). The relative level of nitrosylated GluA1 was obtained by dividing the signal from anti-nitroso-cysteine antibody with the amount of GluA1 immunoprecipitated, and then normalizing it to input. Data are presented as mean ± SEM of fold change versus sham. For the detection of SNO-Histone Deacetylase 2 (HDAC2), anti-nitroso-cysteine antibody, chemically crosslinked with paramagnetic beads, was used to immunoprecipitated samples, in order to avoid the interference of immunoglobulin heavy chain (IgG, 55 KDa). Immunoprecipitated samples were then analyzed by Western blot with the specific anti-HDAC2 antibody (Supplementary Table 1). The relative level of SNO-HDAC2 was obtained dividing the IP signal by the input value.

Enzyme-Linked Immunosorbent Assay Measurements

Brain tissues were obtained as described for Western blot and stored at −80°C. Enzyme-linked immunosorbent assay (ELISA) measurements were performed according to published protocols (Podda et al. 2016). The concentration of BDNF was determined using the Mouse BDNF ELISA Kit (Immunological Science), according to the manufacturer's instructions.

L-NAME Administration

Nω-Nitro-L-arginine methyl ester hydrochloride (L-NAME, Sigma, prod. No. N5751; 25 mg/kg body weight) was diluted in sterile saline solution (i.e., vehicle) and a volume of 10 µL/g body weight was intraperitoneally injected for vehicle and L-NAME solutions. L-NAME or vehicle was administered 3 h prior to each tDCS session or sham stimulation. L-NAME treatment schedule was chosen based on previously published studies, showing that a 2-h treatment is already sufficient to achieve maximal drug distribution in the tissue and more than 50% enzyme inhibition in vivo (Dwyer et al. 1991; Rao and Butterworth 1996).

Two hours after the final stimulation session, mice were sacrificed and tissues processed for molecular analyses (i.e., Western immunoblot and protein nitrosylation assays) or for electrophysiological recordings. Tissues for BDNF evaluation by ELISA were explanted 24 h after 3 × tDCS. Given that statistical analysis revealed no significant effect of vehicle administration on tDCS effects at the molecular level, mEPSC, LTP, and behavioral analyses, were performed only on tDCS- and sham-stimulated mice all injected with L-NAME.

Single-Pellet Reaching Task

The effect of tDCS on skilled reaching movements was evaluated by the single-pellet reaching task, according to published protocols (Chen et al. 2014). From 2 days before, and during the whole experimental period, animals were food restricted to achieve approximately 90% of their free-feeding weights. Animals underwent a gradual 3-day "acclimatization" period to get familiar with both the training chamber and the seeds. In particular, on day 1, two mice were put at the same time into a Plexiglas box for 15 min with food pellets initially available (~20 seeds/mouse) inside the cage (namely, group habitat acclimatization). On day 2, mice were placed into the training chamber individually (namely, individual habitat acclimatization) with seeds available as in day 1. Pellets were then gradually removed from the floor and placed farther away on the shelf until the mice were forced to reach and retrieve the food pellets (Day 3). The pellets were placed in the central indentations, allowing the mice to display their preferred paw and kept in this position for the subsequent 'Shaping' phase, which lasted 3 days. The shaping phase finished when the mouse performed 20 reaching attempts within 15 min and more than 70% reaches with its preferred forelimb. The pellets were then placed on the side that enabled the use of the preferred forepaw only and each animal was trained to reach 40 pellets each day for 8 days to achieve a stable baseline (training phase). If an animal extended the preferred forelimb through the slit to reach and obtain a food pellet, the reach was scored as a success. If an animal knocked the food away or drop the seed after grasping it, the reach was scored as a miss. Performance was defined by: 1) success rate or percentage of success, which is the number of successful retrievals/40*100 (Farr and Whishaw 2002) and 2) speed of success, which represents the number of successful reaches in a minute. After baseline performance had been established, mice were subjected to 3 × tDCS, or sham stimulation, and their motor function was retested 24 h after the end of the stimulation protocol (Fig. 4A).

Based on data from the literature, effects of anodal tDCS were expected on both motor skill acquisition (i.e., online learning) and consolidation/retention (i.e., offline learning) (Reis et al. 2009). Both aspects of motor learning rely on plasticity mechanisms and, therefore, were eligible for our study. We chose to examine tDCS once skill reaching was achieved to a comparable level in all mice since this paradigm allowed us to: 1) avoid possible confounding factors in evaluating tDCS impact on plasticity due to occluding effects of "online" learning on LTP (Rioult-Pedotti et al. 2000, 2007; Hodgson et al. 2005) and 2) apply tDCS in a time window overlapping with consolidation/retention processes (i.e., during 3 days following the end of the training phase).

Grip Strength

A grip strength meter (GSM, Bioseb Instrument) was used to assess forelimb grip strength. Mice were held by the tail and

allowed to grasp a wire grid with their forepaws. They were then pulled backwards by the tail until they released the grid (Bonetto et al. 2015). Grip strength was expressed as the mouse forelimb force measured in grams by the GSM, divided by grams of body weight. The average of three consecutive attempts was used for statistical analysis.

Statistical analysis

The results are presented as mean ± SEM Statistical analysis was performed using SigmaPlot 14.0 software. Analyses were performed blind. Data were first tested for equal variance and normality (Shapiro–Wilk test). The statistical test used (i.e., Student's *t*-test, Mann–Whitney, Welch's test, one-way and two-way analysis of variance (ANOVA), one-way and two-way repeated measure [RM] ANOVA) is indicated in the main text for each experiment. Post hoc multiple comparisons were performed with Bonferroni and Student–Newman–Keuls (SNK) corrections. All statistical tests were two-tailed and the level of significance was set at 0.05.

Results

Anodal tDCS Enhances Glutamatergic Synaptic Transmission and Plasticity in Layer II/III Pyramidal Neurons of M1

It has been proposed that intrinsic horizontal excitatory synaptic connections within layer II/III are the anatomical substrates for plastic reorganization of motor maps during motor learning and memory. Indeed, strengthening of these connections in the form of LTP or changes in excitatory/inhibitory balance have been demonstrated after skill learning (Hess and Donoghue 1994, 1996; Rioult-Pedotti et al. 1998). Therefore, we assessed whether anodal tDCS enhanced LTP in layer II/III of M1. Slices obtained from mice receiving 3 × tDCS (250 µA for 20 min, once/day for 3 consecutive days) showed LTP values significantly higher than controls (66.6 ± 11.4% [$n = 9$ slices from 6 3 × tDCS mice] vs. 38.3 ± 4.9% [$n = 13$ slices from 6 control mice]; $P = 0.014$; unpaired Student's *t*-test; Fig. 2A,B). Similar results were obtained 1 week after stimulation (57.9 ± 7.4% [$n = 10$ slices from 5 3 × tDCS mice] vs. 35.9 ± 6.2% [$n = 11$ slices from 5 control mice]; $P = 0.026$; unpaired Student's *t*-test; Fig. 2C,D), thus suggesting persisting effects of tDCS on synaptic plasticity in M1. We adopted a triple stimulation protocol since pilot experiments showed that a single 20 min-tDCS session (1 × tDCS), that was effective in enhancing LTP at hippocampal CA3-CA1 synapses (Podda et al. 2016), was not sufficient to affect LTP in M1 (38.8 ± 4.3% [$n = 11$ slices from 4 1 × tDCS mice]; $P = 0.94$ vs. controls, unpaired Student's *t*-test; Supplementary Fig. 2). A subset of LTP recordings at layer II/III following TBS of vertical afferents showed that 3 × tDCS also increased the strength of these synapses (54.9 ± 9.1% [n = 10 slices from 5 3 × tDCS mice] vs. 33.3 ± 5.9% [$n = 11$ slices from 5 control mice]; $P = 0.045$; unpaired Student's *t*-test; Supplementary Fig. 3).

We also measured the strength of synaptic connections within layer II/III and found that fEPSP amplitudes evoked in 3 × tDCS mice at different stimulation intensities were larger than those of control mice (same slices used for LTP recordings; $F_{1,119} = 11.67$, $P = 0.002$, main effect of tDCS treatment; $F_{6,119} = 180.76$, $P < 0.001$, main effect of stimulus intensity; $F_{6,119} = 3.83$, $P = 0.002$, interaction between tDCS and stimulus intensity; two-way RM ANOVA; Fig. 3B). These data suggest that tDCS also affects glutamatergic synaptic transmission in M1.

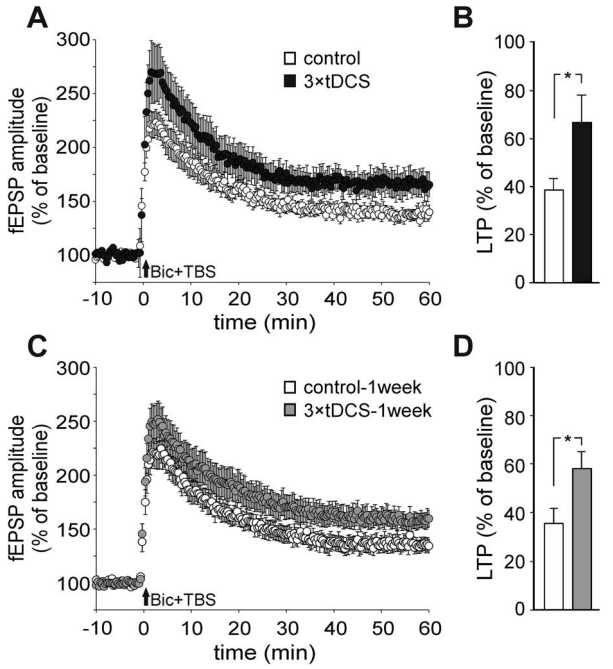

Figure 2. Repeated anodal tDCS sessions (3 × tDCS) enhanced LTP at layer II/III horizontal connections of M1. *A*: Time course of LTP in M1 acute slices from mice sacrificed soon after 3 × tDCS. LTP induction protocol consisted of five TBS delivered every 10 s in the presence of 10 µM bicuculline (Bic). Slices were obtained from sham-stimulated controls ($n = 13$ slices from 6 mice) and mice receiving 3 × tDCS ($n = 9$ slices from 6 mice). Results are expressed as percentages of baseline fEPSP amplitude (mean values for the last 5 min of recording before TBS taken as 100%). *B*: Bar graph comparing LTP measured 55–60 min after TBS, in control and 3 × tDCS mice. *C,D*: Time course (*C*) and magnitude (*D*) of LTP induced by TBS protocol in M1 slices from mice sacrificed 1 week after 3 × tDCS ($n = 10$ slices from 5 mice) or sham stimulation ($n = 11$ slices from 5 mice). Data are expressed as mean ± SEM. *$P < 0.05$.

To further assess the effect of tDCS on glutamatergic transmission, whole-cell voltage-clamp recordings were performed from layer II/III pyramidal neurons. Presynaptic plasticity was examined by analyzing PPR. Paired-pulse facilitation (PPF) was observed in both control and 3 × tDCS mice at 20 and 50 ms interstimulus intervals. However, mice that had undergone 3 × tDCS showed PPR values at 20 ms significantly lower compared to control mice (PPR20: 1.17 ± 0.04 [$n = 21$ cells from 5 3 × tDCS mice] vs. 1.40 ± 0.08 [$n = 18$ cells from 3 control mice]; $P = 0.010$, Welch's test; PPR50: 1.37 ± 0.07 [$n = 18$ cells from 5 3 × tDCS mice] vs. 1.39 ± 0.08 [$n = 19$ cells from 3 control mice]; $P = 0.76$; Mann–Whitney test; Fig. 3C).

The ratio between AMPAR and NMDAR-mediated responses to the stimulation of layer II/III horizontal connections was also estimated. Results showed that the AMPA/NMDA ratio was significantly increased in 3 × tDCS mice compared to sham-stimulated, control mice (1.04 ± 0.09 [$n = 20$ cells from 7 3 × tDCS mice] vs. 0.70 ± 0.08 [$n = 20$ cells from 7 control mice]; $P = 0.004$, Mann–Whitney test; Fig. 3D).

By recording mEPSCs from layer II/III pyramidal neurons, we also found that frequency was increased in slices from 3 × tDCS mice compared to control mice (3.86 ± 0.37 Hz [$n = 21$ cells from 6 3 × tDCS mice] vs. 2.02 ± 0.19 Hz [n = 21 cells from 4 control mice]; $P = 0.001$, Mann–Whitney test; Fig. 3E). No changes were, instead, found in mEPSC amplitudes ($P = 0.71$; Mann–Whitney

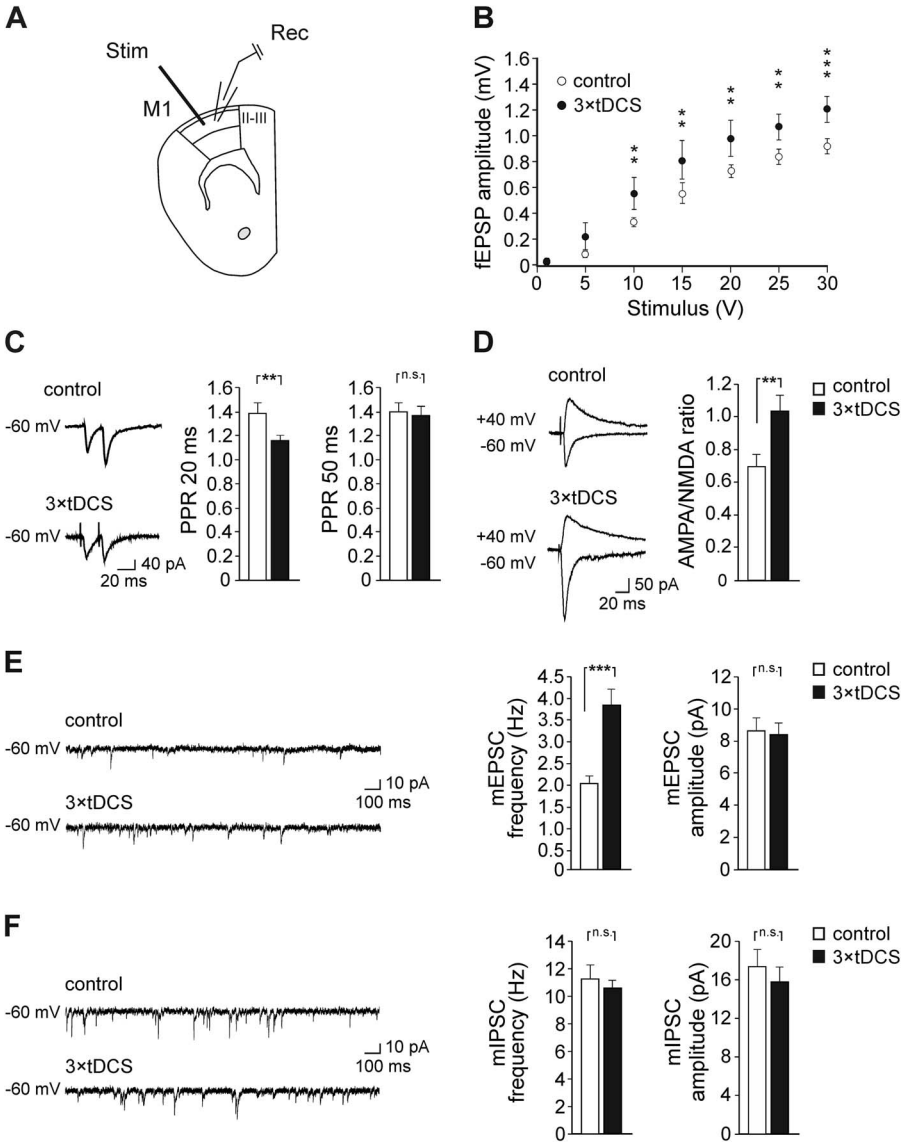

Figure 3. 3 × tDCS enhanced synaptic transmission in M1 layer II/III. *A*: Schematic representation depicting electrode placement during electrophysiological recordings. *B*: fEPSP amplitudes following stimulation of horizontal fibers at layer II/III in M1 at increasing stimulus intensities in slices obtained from control and 3 × tDCS mice (same slices used for LTP; $P = 0.01$ at 10 V, $P = 0.004$ at 15 V; $P = 0.003$ at 20 V; $P = 0.002$ at 25 V; $P < 0.001$ at 30 V; 3 × tDCS vs. control). *C*: Responses to paired-pulse stimulation at 20 and 50 ms interstimulus intervals in slices obtained from control (PPR20: $n = 18$ cells from 3 mice; PPR50: $n = 19$ cells from 3 mice) and 3 × tDCS mice (PPR20: $n = 21$ cells from 5 mice; PPR50: $n = 18$ cells from 5 mice). Representative traces for PPR20 are shown on the left. *D*: Representative AMPAR and NMDAR-mediated responses obtained from stimulation of layer II/III horizontal connections in control and 3 × tDCS mice and bar graph showing AMPA/NMDA ratio ($n = 20$ cells from 7 3 × tDCS mice vs. $n = 20$ cells from 7 control mice). *E*: Bar graphs showing that mEPSC frequency was significantly increased in 3 × tDCS mice compared to control mice, whereas no changes were observed in mEPSC amplitude. Raw traces on the left are representative patch-clamp recordings of mEPSCs. *F*: Raw traces and bar graph showing no changes in mIPSC frequency and amplitude following 3 × tDCS ($n = 18$ cells from 5 3 × tDCS mice vs. $n = 17$ cells from 6 control mice). Data are expressed as mean ± SEM. $^{**}P \leq 0.01$, $^{***}P \leq 0.001$; n.s., not significant.

test; Fig. 3*E*). Increased mEPSC frequency and decreased PPR suggest increased presynaptic glutamate release following 3 × tDCS. Recordings of mIPSCs from layer II/III pyramidal neurons showed no differences in amplitudes and frequency between 3 × tDCS and control groups (frequency: 10.59 ± 0.56 Hz [n = 18 cells from 5 3 × tDCS mice] vs. 11.29 ± 0.96 Hz [$n = 17$ cells from 6 control mice]; $P = 0.51$, unpaired Student's *t*-test; amplitude: 15.84 ± 1.47 Hz [$n = 18$ cells from 5 3 × tDCS mice] vs. 17.44 ± 1.71 Hz [$n = 17$ cells from 6 control mice]; $P = 0.43$, Mann–Whitney test; Fig. 3*F*), thus supporting a specific effect of tDCS on glutamatergic transmission.

Anodal tDCS Enhances Forelimb Skilled Motor Performance and Increases Spine Density in the M1

Next, we assessed the effects of the 3 × tDCS protocol on forelimb motor performance in a skilled reaching task. Mice were trained in a plexiglass box to extend their preferred paw through a slit in the front wall in order to grasp individual food pellets as described in Methods (Fig. 4*B*). After baseline performance had been established, mice were randomly assigned to control or 3 × tDCS groups ($n = 10$ mice for each group). Mice were retested in the "single-pellet reaching task" 24 h after 3 × tDCS

or sham stimulation. In control mice, no significant changes were observed 24 h after sham stimulation in both performance indices analyzed (success rate: 38.9 ± 2.8% vs. 39.9 ± 3.8% baseline values at the end of training; $P = 0.74$; speed of success: 1.89 ± 0.19 vs. 1.66 ± 0.22 baseline values; $P = 0.31$; paired Student's *t*-test; Fig. 4C,D). Following 3 × tDCS, both indices were, instead, significantly enhanced with respect to either baseline values (success rate: 53.7 ± 2.7% vs. 43.0 ± 4.4%; $P = 0.002$; speed of success 2.79 ± 0.21 vs. 1.63 ± 0.21; $P = 0.0009$; paired Student's *t*-test, Fig. 4C,D) and to values obtained in control mice ($P = 0.001$ for success rate and $P = 0.005$ for speed of success; unpaired Student's *t*-test; Fig. 4C,D). These data indicate that tDCS improved already acquired motor skills.

We also measured the effect of 3 × tDCS on forelimb strength—an important outcome measure in clinical practice. Interestingly, 3 × tDCS mice ($n = 9$) showed a significant enhancement of muscle strength 24 h after stimulation, as revealed by GSM, with respect to prestimulation baseline values (4.45 ± 0.21 vs. 3.88 ± 0.18 g/g prestimulation baseline values; $P = 0.000008$; paired Student's *t*-test; Fig. 4E) and values obtained in control mice ($n = 9$) after sham stimulation ($P = 0.006$, unpaired Student's *t*-test; Fig. 4E). No significant changes in forelimb strength were, instead, observed after sham stimulation (3.80 ± 0.09 vs. 3.99 ± 0.17 g/g; $P = 0.28$; paired Student's *t*-test; Fig. 4E).

Since motor learning and consolidation of motor memories have been associated to long-lasting synaptic reorganization in the M1 (Xu et al. 2009) and tDCS was previously shown to affect structural plasticity in other experimental models (Paciello et al. 2018), we evaluated the effect of 3 × tDCS on spine density in the M1. Morphological analysis performed on a total of 80 pyramidal neurons belonging to M1 layer II/III (40 pyramidal neurons per group; $n = 4$ mice for each group), revealed that 3 × tDCS significantly increased spine density in both apical and basal dendrites (apical dendrites: $F_{1,78} = 33.97$; $P < 0.001$; basal dendrites: $F_{1,78} = 27.14$; $P < 0.001$ 3 × tDCS vs. control group; one-way RM ANOVA (group × dendrites); Fig. 4F,G).

Anodal tDCS Affects Molecular Determinants of Synaptic Plasticity

Finally, we sought to identify the molecular determinants of the tDCS effects observed at electrophysiological, morphological, and behavioral levels.

In particular, we evaluated the levels of $pCREB^{Ser133}$ and CaMKII phosphorylation at Thr286 ($pCaMKII^{Thr286}$), since they are well-known components of the intracellular cascade subtending LTP expression (Herring and Nicoll 2016) and have been linked to tDCS effects in other brain areas (Podda et al. 2016; Kim et al. 2017; Stafford et al. 2018). Phosphorylation of AMPA receptor (AMPAR) GluA1 subunit at Ser831 was also evaluated in our experimental conditions because of its role in AMPAR function and trafficking. Interestingly, GluA1 phosphorylation at Ser831 by CaMKII is required for receptor trafficking into the postsynaptic membrane during hippocampal LTP (Barria et al. 1997; Kristensen et al. 2011) and it is enhanced in the motor cortex during motor skill learning (Kida and Mitsushima 2018). Our Western immunoblot analyses performed on motor cortex extracts from 3 × tDCS ($n = 7$) and control mice ($n = 6$) revealed that 3 × tDCS significantly increased the levels of $pCREB^{Ser133}$ (+101% vs. control; $P = 0.002$), $pCaMKII^{Thr286}$ (+85% vs. controls; $P = 0.031$) and $pGluA1^{Ser831}$ (+146% vs. control; $P = 0.037$; one-way ANOVA; Fig. 5A).

It has been recently shown that nitric oxide (NO)-dependent GluA1 S-nitrosylation enhances $pGluA1^{Ser831}$ and increases single-channel conductance (Selvakumar et al. 2013). NO attracted our attention as a potential candidate in mediating tDCS effects since its production, via neuronal NO synthase (nNOS) activation, would be consistent with the role of tDCS in promoting intracellular Ca^{2+} increases (Pelletier and Cicchetti 2014; Rohan et al. 2015). Therefore, we analyzed GluA1 S-nitrosylation in the motor cortex extracts from mice sacrificed 2 h after sham stimulation or 3 × tDCS ($n = 6$ for each group). Results revealed increased levels of GluA1 S-nitrosylation in 3 × tDCS mice when compared to controls (+202% vs. controls; $P = 0.008$; unpaired Student's *t*-test; Fig. 5B), suggesting that NO signaling is activated by tDCS. To establish a causal link between the increased levels of $pGluA1^{Ser831}$ and NO-mediated S-nitrosylation of GluA1, we treated mice with the NOS inhibitor L-NAME (25 mg/kg body weight, see Methods). Results showed that treatment with L-NAME prevented the tDCS-induced increase in $pGluA1^{Ser831}$ levels ($n = 4$ mice for each group; $P = 0.58$, 3 × tDCS-L-NAME vs. L-NAME control mice; two-way ANOVA, Bonferroni post hoc), whereas significant enhancement of $pGluA1^{Ser831}$ was confirmed in 3 × tDCS mice that received vehicle injection (+71.0% vs. vehicle-injected controls [$n = 4$ for each group]; $P = 0.001$; two-way ANOVA, Bonferroni post hoc; Fig. 5C). Overall, two-way ANOVA showed a main effect of either 3 × tDCS ($F_{1,15} = 29.6$; $P = 0.001$) or L-NAME ($F_{1,15} = 22.8$; $P = 0.001$) and an interaction between 3 × tDCS and L-NAME ($F_{1,15} = 22.8$; $P = 0.002$), strongly supporting the activation of NO pathway by tDCS.

Based on our previous study (Podda et al. 2016) and the aforementioned molecular data, our analysis of possible NO-mediated tDCS effects was extended to BDNF. In particular, we hypothesized that tDCS affected the level of BDNF in M1 via NO-mediated S-nitrosylation of HDAC2. Indeed, we previously showed that anodal tDCS epigenetically regulates BDNF expression in the hippocampus via a $pCREB^{Ser133}$-mediated recruitment of the histone acetyltransferase CBP on *Bdnf* promoter I, with consequent increase in H3 acetylation at lysine 9. However, the expression of BDNF not only relies on CBP activation, but also on the inhibition of repressors such as HDAC2 (Hsiao et al. 2017; Sartor et al. 2019) whose activity is negatively regulated by S-nitrosylation (Colussi et al. 2008; Nott et al. 2008). It is worth noting that our IP experiments revealed increased levels of HDAC2 S-nitrosylation in 3 × tDCS mice when compared to controls (+67.3% vs. control [n = 4 mice for each group]; $P = 0.002$) and this effect was prevented by L-NAME (L-NAME-injected 3 × tDCS mice [$n = 5$] vs. vehicle-injected 3 × tDCS mice [$n = 4$]; $P = 0.01$; two-way ANOVA, Bonferroni post hoc; Fig. 6A). ELISA measurements showed that, in mice subjected to 3 × tDCS, BDNF levels were higher (+67%) than in controls (96.3 ± 11.9 pg/mg vs. 57.6 ± 9.34 pg/mg [$n = 4$ mice for each group]; $P = 0.02$; two-way ANOVA, SNK post hoc; Fig. 6B). A tDCS-induced increase of BDNF levels was prevented by treatment of mice with L-NAME (71.2 ± 4.1 pg/mg in L-NAME-injected 3 × tDCS mice vs. 64.8 ± 3.3 pg/mg in L-NAME-injected sham-stimulated controls [$n = 4$ mice for each group]; $P = 0.04$; two-way ANOVA, SNK post hoc; Fig. 6B).

Finally, we investigated the role of NO signaling in the tDCS-induced modulation of synaptic function and motor behavior by reassessing the effect of 3 × tDCS on mEPSCs, LTP and success rate in mice treated with L-NAME. We found that L-NAME prevented 3 × tDCS effects on mEPSC frequency (2.80 ± 0.27 Hz [$n = 17$ cells from 3 3 × tDCS mice] vs. 2.17 ± 0.22 Hz [$n = 16$ cells

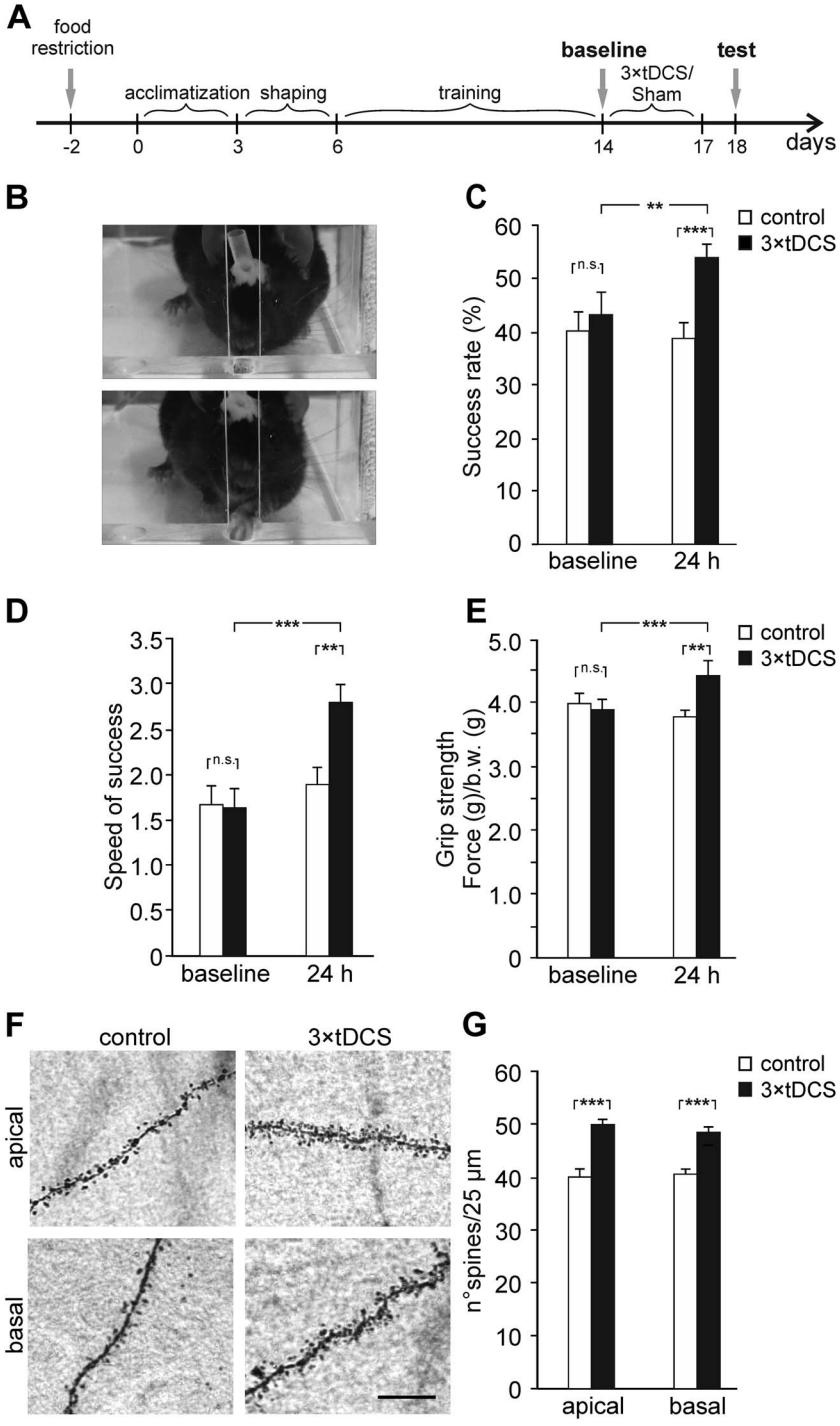

Figure 4. 3 × tDCS enhanced forelimb motor skill and strength and increased spine density in the M1. *A*: Timeline of single-pellet reaching test and tDCS schedule. *B*: Photographs showing a mouse implanted with a tDCS electrode, performing the single-pellet reaching task. *C*,*D*: Reaching success (*C*) and speed of success (*D*) were increased in mice subjected to 3 × tDCS compared to sham-stimulated control mice ($n = 10$ mice/each group), 24 h after the end of stimulation protocol. No significant changes were observed in both indices in control mice tested 24 h after sham stimulation. *E*: Bar graph showing that forelimb strength was enhanced by 3 × tDCS ($n = 9$ mice/each group); b.w., body weight. *F*: Representative images of apical and basal dendrites of M1 layer II/III pyramidal neurons in control and 3 × tDCS mice ($n = 4$ mice/each group). Scale bar: 10 µm. *G*: Bar graph showing mean values of spine density in all neurons examined (40 neurons per group). Data are expressed as mean ± SEM. $^{**}P \leq 0.01$, $^{***}P \leq 0.001$; n.s., not significant.

from 3 control mice]; $P = 0.14$; two-way ANOVA, Bonferroni post hoc; Fig. 6C). Overall, comparison by ANOVA of data obtained from L-NAME-treated and non-treated mice revealed a statistically significant interaction between 3 × tDCS and L-NAME treatments ($F_{1,71} = 4.512$, $P = 0.037$). Similarly, L-NAME treatment hindered 3 × tDCS effects on LTP (45.2 ± 6.6% [$n = 9$ slices from 6 L-NAME-injected 3 × tDCS mice] vs. 39.5 ± 2.2% [$n = 8$ slices from 5 L-NAME-injected control mice]; $P = 0.57$;

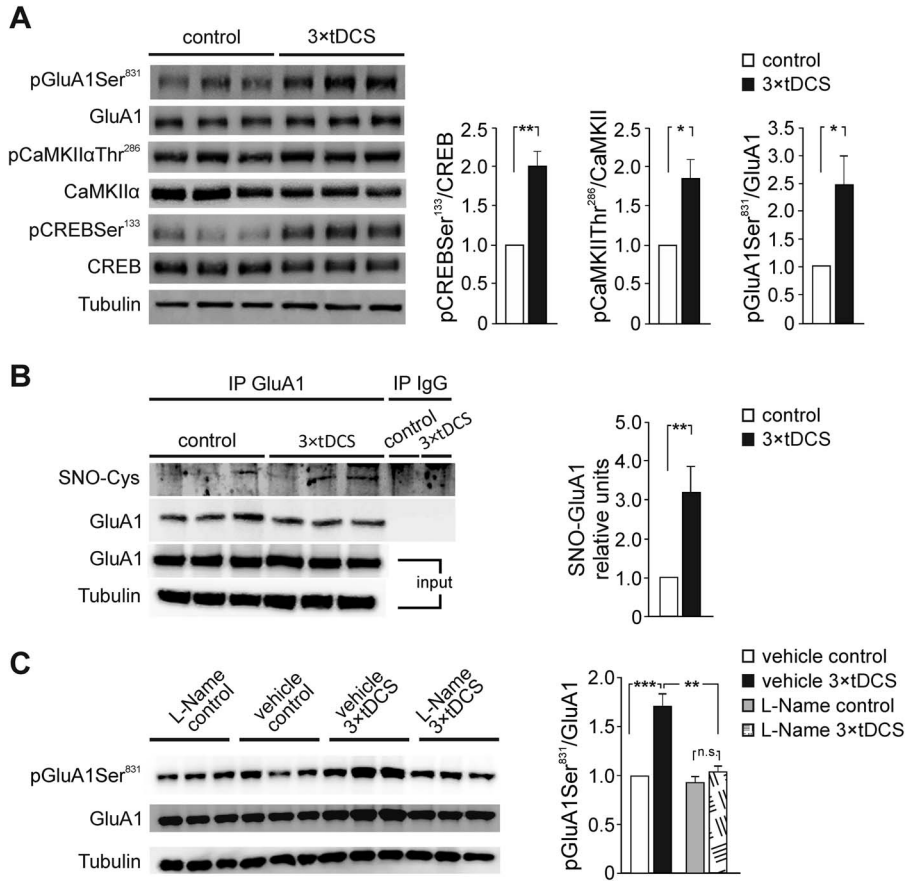

Figure 5. Molecular changes occurring in the mouse motor cortex following 3 × tDCS. *A*: Representative immunoblots revealing increased pCREB^{Ser133}, pCaMKII^{Thr286}, and pGluA1^{Ser831} levels following 3 × tDCS. Bar graphs show results of densitometric analyses on all samples ($n = 6$ control and $n = 7$ 3 × tDCS mice) normalized to both the corresponding total protein level and tubulin. *B*: Representative immunoprecipitation experiments showing GluA1 S-nitrosylation (SNO-GluA1) assessed by Western blotting. A pool of three samples was used in each negative control for IgG immunoprecipitation. Input values for GluA1 and tubulin are shown in the lower panel. Densitometric analysis relative to input shows that GluA1 S-nitrosylation is increased in the motor cortex from 3 × tDCS-mice, compared to controls ($n = 6$ mice/each group). The relative level of SNO-GluA1 is expressed as mean ± s.e.m. of fold change vs. control, taken as 1. *C*: Representative immunoblots and results of densitometric analysis showing that, in the presence of the NOS inhibitor, L-NAME, tDCS failed to increase pGluA1^{Ser831} ($n = 4$ mice/each group). Data are expressed as mean ± SEM. $^{*}P < 0.05$, $^{**}P \leq 0.01$; n.s., not significant.

two-way ANOVA, Bonferroni post hoc; Fig. 6*D*) and success rate (36.8 ± 7.4% vs. 35.0 ± 5.3% with respect to baseline values [$n = 7$ L-NAME-injected 3 × tDCS mice; $P = 0.66$] and to values obtained in L-NAME-injected control mice [$n = 6$], $P = 1$; two-way RM ANOVA, Bonferroni post hoc; Fig. 6*E*), confirming the involvement of NO signaling in mediating tDCS effects in our experimental model.

Discussion

Here we report that repeated sessions of anodal tDCS, over the mouse M1 area, enhanced LTP and glutamatergic synaptic transmission at layer II/III horizontal connections. At the behavioral level, 3 × tDCS protocol resulted in improvement of already acquired skills and enhanced forelimb strength. Molecular analyses showed that tDCS modulates plasticity-related pathways and revealed a novel key role for NO as a mediator of tDCS effects.

For tDCS, we used an electrode montage and current density similar to those recently adopted for rodent models and close to the recommended safety limits in rodents (Rohan et al. 2015; Podda et al. 2016; Jackson et al. 2017; Paciello et al. 2018; Yu et al. 2018). Specifically, we applied tDCS at 35.4 A/m^2 (250 μA/7.06 mm^2 for 20 min) and found that it did not produce histological lesions in the cortical region underneath the epicranial cannula, as assessed by hematoxylin–eosin staining. Nonetheless, differences between our protocol and typical human tDCS should be taken into consideration when comparing our findings to clinical studies. TDCS protocols in humans usually apply ~0.096 A/m^2 to the cortex with a predicted 0.35 V/m electric field (Datta et al. 2009; Bikson et al. 2016). Rodent epicranial stimulation uses higher currents and is regarded as a "hypersensitive model", compared to human montages. In particular, it is estimated that current density across the mouse brain, in our experimental conditions, is about 2 orders of magnitude greater than human tDCS (i.e., ~7A/m^2 vs. 0.1 A/m^2 in humans). Additionally, obvious differences between mouse and human cortical architecture (i.e., the absence/presence of gyri) would affect the orientation of electric field with respect to somatodendritic axis of M1 neurons and the polarization of cellular compartments. In this regard, based on an in vitro model (Rahman et al. 2013), we expect that tDCS in our experimental model would result in a constant electric field mainly parallel (radial component) to the

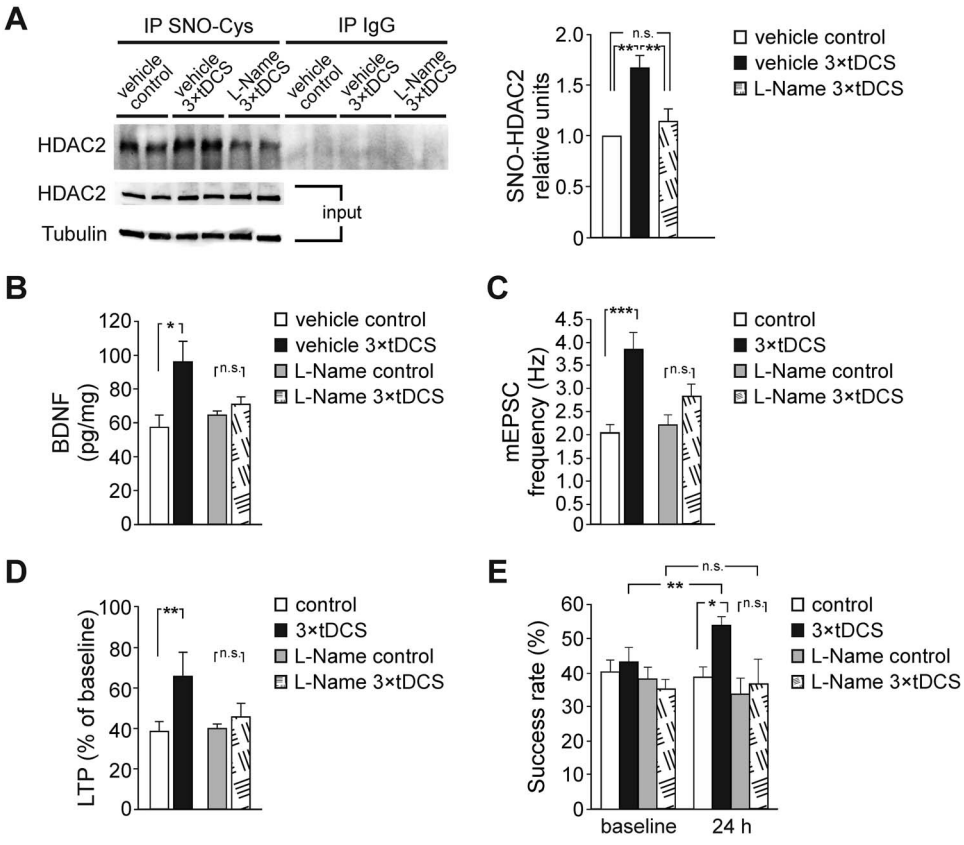

Figure 6. Anodal tDCS activates NO-dependent pathways. *A*: Analysis of HDAC2 nitrosylation. Following 3 × tDCS, the levels of SNO-HDAC2 were increased and this effect was abolished by L-NAME ($n = 5$ mice/each group). Two representative samples for each condition are shown. The relative level of SNO-HDAC2 is expressed as mean ± s.e.m. of fold change vs. control. *B*: Results from ELISA showing that BDNF levels were increased 24 h after 3 × tDCS, and this effect was significantly reduced by L-NAME ($n = 4$ mice/each group). *C*: Bar graphs showing that L-NAME prevented the tDCS-induced increase in mEPSC frequency ($n = 17$ cells from 3 3 × tDCS mice vs. $n = 16$ cells from 3 control mice). *D*: Bar graph showing that L-NAME hindered 3 × tDCS effects on LTP, measured 55–60 min after TBS. Slices were obtained from L-NAME-injected control mice ($n = 8$ slices from 5 mice) and L-NAME injected mice receiving 3 × tDCS ($n = 9$ slices from 6 mice). *E*: Mice treated with L-NAME and subjected to 3 × tDCS ($n = 7$) did not show increased success rate compared to L-NAME injected mice receiving sham stimulation ($n = 6$). Data on 3 × tDCS effects in the absence of L-NAME (i.e, control and tDCS groups), already presented in Figures 2B, 3E, and 4C, respectively, are shown here for a better comparison. All data are expressed as mean ± s.e.m. $^{*}P < 0.05$, $^{**}P \leq 0.01$, $^{***}P \leq 0.001$; n.s., not significant.

somatodendritic axis of pyramidal neurons, producing somatic depolarization. In contrast, in typical human tDCS, both radial and tangential direction currents are induced—the latter being most prevalent across the cortex.

It is worth noting that several cellular and molecular plastic changes elicited by 3 × tDCS in the M1 resemble those underlying motor skill learning (Kida et al. 2016).

As far as LTP is concerned, motor skill learning is believed to induce an LTP-like mechanism, moving the overall population synaptic weight closer to saturation, as suggested by occlusion of subsequent LTP induction (Rioult-Pedotti et al. 2000, 2007; Hodgson et al. 2005). Here we showed that prior treatment of mice with 3 × tDCS did not occlude but, instead, enhanced LTP elicited by TBS protocol 2 to 6 h later. This finding suggests a metaplastic-like effect of tDCS (Abraham and Bear 1996; Abraham and Tate 1997), corroborating recent data obtained in the hippocampus (Ranieri et al. 2012; Rohan et al. 2015; Podda et al. 2016; Kronberg et al. 2017; Cocco et al. 2018; Yu et al. 2018).

Our experimental protocol involving extracellular stimulation of layer II/III was designed to recruit horizontal connections closest to the recording electrodes (~200 µm apart), according to previous published papers (Hess and Donoghue 1994, 1996; Rioult-Pedotti et al. 1998). Nevertheless, we cannot exclude that other afferents, including long range-horizontal connections (Wolters et al. 2003) or vertical afferents might be stimulated in our experiments. In this regard, we found that TBS of vertical inputs, recruited by placing the stimulating electrode in layer V, elicited reliable LTP at layer II/III that was affected by 3 × tDCS, suggesting that these afferents might contribute to the effects on plasticity and synaptic transmission we observed in our study. Further studies by using, for instance, optogenetic analyses are needed to dissect subsets of synapses within layer II/III affected or unaffected by tDCS.

The mechanisms responsible for LTP involve changes at both pre- and postsynaptic sites (MacDougall and Fine 2013) and the results of our electrophysiological and molecular analyses suggest that tDCS exerts its effect at both sites. Specifically, we found that 3 × tDCS enhanced basal synaptic transmission, as inferred from analysis of I/O curves. Similar results were obtained in previous studies following DCS of the motor cortex in brain slices (Fritsch et al. 2010), and following acquisition of new motor skills (Rioult-Pedotti et al. 1998). We found that 3 × tDCS attenuated PPF—a short-term form of synaptic plasticity primarily due to increased presynaptic glutamate release under the influence of residual calcium (Christie and Abraham 1994; Schulz et al. 1994)—at M1 layer II/III horizontal connec-

tions. This is consistent with data from Márquez-Ruiz et al. (2012) showing reduction of PPF in the somatosensory cortex following anodal tDCS. Increased PPF or no changes in this parameter following anodal tDCS were, instead, reported by other studies on hippocampal CA3-CA1 synapses (Rohan et al. 2015; Podda et al. 2016). Such discrepancy might be related to differences in the probability of initial release, which is low in the hippocampus (Abbott and Regehr 2004) and high in the neocortex (Silver et al. 2003). High release probability of M1 synapses might also have hindered tDCS effects at 50 ms interval.

Consistent with an increased rate of glutamate vesicle release, we found enhanced frequency of mEPSCs in slices from 3 × tDCS mice. In our experimental model, no changes in mIPSCs frequency and amplitude were observed, indicating that action potential-independent release of GABA is not affected by 3 × tDCS.

Increases in neurotransmitter release following 3 × tDCS provide a potential mechanism for enhanced LTP expression at M1 glutamatergic synapses. However, increased responsiveness of postsynaptic cells to released glutamate might also account for such effect. Indeed, AMPA/NMDA ratio was significantly increased in 3 × tDCS mice. This result is consistent with the increased spine density we observed following 3 × tDCS.

Consistent with 3 × tDCS effects at postsynaptic sites, molecular analyses showed that the levels of $pCREB^{Ser133}$, $pCaMKII^{Thr286}$, and $pGluA1^{Ser831}$ were all enhanced in the motor cortex of 3 × tDCS mice.

Our data are in line with previous reports showing increased $pCREB^{Ser133}$ and $pGluA1^{Ser831}$ following anodal tDCS of the hippocampus (Podda et al. 2016; Stafford et al. 2018). Since GluA1 Ser831 residue is a CaMKII target, it is plausible that the enhanced $pGluA1^{Ser831}$ we observed in the motor cortex is causally linked to tDCS-induced activation of CaMKII. Phosphorylation of Ser831 is critical for trafficking of AMPARs into the postsynaptic membrane during LTP (Barria et al. 1997; Hayashi et al. 2000; Lu et al. 2010; Kristensen et al. 2011).

Noteworthy, molecular changes similar to those we detected, occur in the hippocampus following Ca^{2+} rise during NMDAR-dependent LTP (Rebola et al. 2010) and in the motor cortex during motor training (Kida et al. 2016; Kida and Mitsushima 2018). Ca^{2+} influx through NMDARs also triggers nNOS activation and NO production (Brenman et al. 1996). Given the well-established role of NO in the modulation of glutamatergic synaptic transmission and plasticity, and the involvement of NMDAR/Ca^{2+} signaling in mediating tDCS effects (Pelletier and Cicchetti 2014; Rohan et al. 2015), we tested the hypothesis that NO contributed to tDCS actions on the motor cortex. To the best of our knowledge, our results provide the first evidence that tDCS activates a NO-dependent pathway in the motor cortex. Specifically, we found that 3 × tDCS enhanced GluA1 S-nitrosylation and, more importantly, we highlighted a causative link between tDCS-promoted GluA1 S-nitrosylation and increased $pGluA1^{Ser831}$, by showing that mouse treatment with the NOS inhibitor, L-NAME, abolished tDCS-induced increases of $pGluA1^{Ser831}$.

Further studies are needed to characterize the contribution of S-nitrosylation of GluA1, and of other synaptic proteins, to regulation of glutamate signaling and plasticity in M1. However, we expected that this post-translational modification boosts synaptic plasticity as observed in other models (Barria et al. 1997; Hayashi et al. 2000; Kristensen et al. 2011; Selvakumar et al. 2013; Santos et al. 2015; von Ossowski et al. 2017). The role of NO as crucial mediator of tDCS action on M1 is strongly supported by results showing that L-NAME treatment prevented tDCS effects at electrophysiological and behavioral levels. In particular, treatment with L-NAME abolished tDCS-promoted increase in mEPSC frequency, indicating that NO is also involved in mediating tDCS effects at presynaptic level. Such effect is fully consistent with NO role as retrograde messenger acting on presynaptic terminals (Lonart et al. 1992). TDCS-induced increase of LTP and success rate were not observed following L-NAME treatment, suggesting causal relationship between effects on plasticity and performance. Remarkably, L-NAME prevented tDCS-induced increase of BDNF levels. BDNF is a highly activity regulated neurotrophin that is crucially involved in hippocampal LTP and hippocampal-dependent learning and memory (Karpova 2014). It has also been implicated in motor cortex plasticity, motor learning and functional recovery after stroke (Cheeran et al. 2008; Fritsch et al. 2010; McHughen et al. 2010). Our data showing that BDNF levels were increased in the motor cortex of 3 × tDCS mice are fully consistent with a large body of evidence implicating BDNF in the response to tDCS, in both humans and rodents (Fritsch et al. 2010; Podda et al. 2016; Wu et al. 2017; Cocco et al. 2018; Paciello et al. 2018; Yu et al. 2018). With regard to the molecular mechanism linking NO production and BDNF expression following tDCS, we propose that S-nitrosylation of HDAC2 may have a critical role. HDAC2 is known to bind the promoter region of genes implicated in plasticity and neuronal activity, such as *Bdnf*, thus repressing their transcription (Hsiao et al. 2017; Sartor et al. 2019). We found that the levels of HDAC2 S-nitrosylation were higher in the motor cortex of 3 × tDCS mice compared to vehicle-injected controls. Given the well-recognized inhibitory role of this modification (Colussi et al. 2008; Nott et al. 2008), S-nitrosylation of HDAC2 may expectedly contribute to the enhanced expression of BDNF we observed in our experimental model. This effect likely cooperated with other tDCS-induced mechanisms leading to enhanced BDNF expression, including the pCREB-dependent recruitment of the histone acetyltransferase, CBP, at the promoter region of the BDNF gene that we previously reported in the hippocampus (Podda et al. 2016).

Taking together results of molecular and electrophysiological analyses, we posit that tDCS boosts synaptic plasticity by "priming" signaling pathways engaged during LTP. The engagement of pre- and postsynaptic mechanisms by tDCS is supported by a recent in vitro study showing changes in presynaptic and/or postsynaptic firing rate during DCS of M1—predicted to increase the coincidence probability and the likelihood for synaptic strengthening (Rahman et al. 2017).

TDCS-induced metaplastic-like effects in the M1 could well account for the behavioral effects that we observed in our study and that many other authors have previously reported in rodent models and humans (Reis et al. 2008, 2009; Roji et al. 2015; Buch et al. 2017; Lefebvre and Liew 2017; Angius et al. 2018). In particular, here we showed that daily 20 min-sessions of anodal tDCS for 3 consecutive days, improved motor skill performance that had been already acquired through practice, reaching a steady level over 8 days of training. This result suggests an effect of tDCS on the process of consolidation that occurs "offline" and has been implicated in motor memory retention over time (Robertson et al. 2005). Of note, it has been suggested that prolonged persistence of learning-induced synapses might be a mechanism for the consolidation of motor memories (Xu et al. 2009) and we recently demonstrated that anodal tDCS increased the number of both stable, mushroom-type, and newly-formed, thin-type, spines in the auditory cortex through a BDNF/TrkB-mediated mechanism (Paciello et al. 2018). In keeping with these

findings, our morphological analysis in the M1 revealed that, 24 h after the end of tDCS protocol, spine density was increased in both apical and basal dendrites of layer II/III pyramidal neurons. Coordinated recruitment of intracortical synapses onto corticospinal neurons, as a result of the enhancement in the number or strength of synapses, would be also a plausible mechanism subtending the enhanced forelimb strength documented here.

Collectively, our results corroborate the emerging view of tDCS-induced metaplastic-like effects and strongly support its use to improve motor functions under physiological conditions and to promote motor recovery after stroke.

Supplementary Material

Supplementary material is available at *Cerebral Cortex* online.

Funding

Office of Naval Research Global (grant N62909–15-1-2002); Fondazione Roma (grant NCDS-2013-00000349); and D1 intramural funds from Università Cattolica.

Notes

Conflict of Interest: None declared.

References

Abbott LF, Regehr WG. 2004. Synaptic computation. *Nature*. 431:796–803.

Abraham WC, Bear MF. 1996. Metaplasticity: the plasticity of synaptic plasticity. *Trends Neurosci*. 19:126–130.

Abraham WC, Tate WP. 1997. Metaplasticity: a new vista across the field of synaptic plasticity. *Prog Neurobiol*. 52:303–323.

Angius L, Mauger AR, Hopker J, Pascual-Leone A, Santarnecchi E, Marcora SM. 2018. Bilateral extracephalic transcranial direct current stimulation improves endurance performance in healthy individuals. *Brain Stimul*. 11:108–117.

Barria A, Muller D, Derkach V, Griffith LC, Soderling TR. 1997. Regulatory phosphorylation of AMPA-type glutamate receptors by CaM-KII during long-term potentiation. *Science*. 276:2042–2045.

Bikson M, Grossman P, Thomas C, Zannou AL, Jiang J, Adnan T, Mourdoukoutas AP, Kronberg G, Truong D, Boggio P *et al*. 2016. Safety of Transcranial direct current stimulation: evidence based update 2016. *Brain Stimul*. 9:641–661.

Bonetto A, Andersson DC, Waning DL. 2015. Assessment of muscle mass and strength in mice. *Bonekey Rep*. 4:732.

Brasil-Neto JP. 2012. Learning, memory, and transcranial direct current stimulation. *Front Psych*. 3:80.

Brenman JE, Chao DS, Gee SH, McGee AW, Craven SE, Santillano DR, Wu Z, Huang F, Xia H, Peters MF *et al*. 1996. Interaction of nitric oxide synthase with the postsynaptic density protein PSD-95 and alpha1-syntrophin mediated by PDZ domains. *Cell*. 84:757–767.

Buch ER, Santarnecchi E, Antal A, Born J, Celnik PA, Classen J, Gerloff C, Hallett M, Hummel FC, Nitsche MA *et al*. 2017. Effects of tDCS on motor learning and memory formation: a consensus and critical position paper. *Clin Neurophysiol*. 128:589–603.

Cambiaghi M, Velikova S, Gonzalez-Rosa JJ, Cursi M, Comi G, Leocani L. 2010. Brain transcranial direct current stimulation modulates motor excitability in mice. *Eur J Neurosci*. 31:704–709.

Castro-Alamancos MA, Donoghue JP, Connors BW. 1995. Different forms of synaptic plasticity in somatosensory and motor areas of the neocortex. *J Neurosci*. 15:5324–5333.

Cheeran B, Talelli P, Mori F, Koch G, Suppa A, Edwards M, Houlden H, Bhatia K, Greenwood R, Rothwell JC. 2008. A common polymorphism in the brain-derived neurotrophic factor gene (BDNF) modulates human cortical plasticity and the response to rTMS. *J Physiol*. 586:5717–5725.

Chen C, Gilmore A, Zuo Y. 2014. Study motor skill learning by single-pellet reaching tasks in mice. *J Vis Exp*. 85:e51238.

Christie BR, Abraham WC. 1994. Differential regulation of paired-pulse plasticity following LTP in the dentate gyrus. *Neuroreport*. 5:385–388.

Cirillo G, Di Pino G, Capone F, Ranieri F, Florio L, Todisco V, Tedeschi G, Funke K, Di Lazzaro V. 2017. Neurobiological after-effects of non-invasive brain stimulation. *Brain Stimul*. 10:1–18.

Cocco S, Podda MV, Grassi C. 2018. Role of BDNF signaling in memory enhancement induced by transcranial direct current stimulation. *Front Neurosci*. 12:427.

Colussi C, Mozzetta C, Gurtner A, Illi B, Rosati J, Straino S, Ragone G, Pescatori M, Zaccagnini G, Antonini A *et al*. 2008. HDAC2 blockade by nitric oxide and histone deacetylase inhibitors reveals a common target in Duchenne muscular dystrophy treatment. *Proc Natl Acad Sci U S A*. 105:19183–19187.

Datta A, Bansal V, Diaz J, Patel J, Reato D, Bikson M. 2009. Gyri-precise head model of transcranial direct current stimulation: improved spatial focality using a ring electrode versus conventional rectangular pad. *Brain Stimul*. 2:201–207.

Dwyer MA, Bredt DS, Snyder SH. 1991. Nitric oxide synthase: irreversible inhibition by L-NG-nitroarginine in brain in vitro and in vivo. *Biochem Biophys Res Commun*. 176:1136–1141.

Farr TD, Whishaw IQ. 2002. Quantitative and qualitative impairments in skilled reaching in the mouse (Mus musculus) after a focal motor cortex stroke. *Stroke*. 33:1869–1875.

Franklin KBJ, Paxinos GT. 1997. *The Mouse Brain in Stereotaxic Coordinates*. New York: Academic Press.

Fritsch B, Reis J, Martinowich K, Schambra HM, Ji Y, Cohen LG, Lu B. 2010. Direct current stimulation promotes BDNF-dependent synaptic plasticity: potential implications for motor learning. *Neuron*. 66:198–204.

Hayashi Y, Shi SH, Esteban JA, Piccini A, Poncer JC, Malinow R. 2000. Driving AMPA receptors into synapses by LTP and CaMKII: requirement for GluR1 and PDZ domain interaction. *Science*. 287:2262–2267.

Herring BE, Nicoll RA. 2016. Long-term potentiation: from CaMKII to AMPA receptor trafficking. *Annu Rev Physiol*. 78:351–365.

Hess G, Donoghue JP. 1994. Long-term potentiation of horizontal connections provides a mechanism to reorganize cortical motor maps. *J Neurophysiol*. 71:2543–2547.

Hess G, Donoghue JP. 1996. Long-term potentiation and long-term depression of horizontal connections in rat motor cortex. *Acta Neurobiol Exp (Wars)*. 56:397–405.

Hodgson RA, Ji Z, Standish S, Boyd-Hodgson TE, Henderson AK, Racine RJ. 2005. Training-induced and electrically induced potentiation in the neocortex. *Neurobiol Learn Mem*. 83: 22–32.

Hsiao YH, Hung HC, Yu YJ, Su CL, Chen SH, Gean PW. 2017. Co-housing reverses memory decline by epigenetic regulation of brain-derived neurotrophic factor expression in an animal model of Alzheimer's disease. *Neurobiol Learn Mem*. 141:1–8.

Jackson MP, Rahman A, Lafon B, Kronberg G, Ling D, Parra LC, Bikson M. 2016. Animal models of transcranial direct current stimulation: methods and mechanisms. *Clin Neurophysiol*. 127:3425–3454.

Jackson MP, Truong D, Brownlow ML, Wagner JA, McKinley RA, Bikson M, Jankord R. 2017. Safety parameter considerations of anodal transcranial direct current stimulation in rats. *Brain Behav Immun*. 64:152–161.

Karpova NN. 2014. Role of BDNF epigenetics in activity-dependent neuronal plasticity. *Neuropharmacology*. 76:709–718.

Kida H, Tsuda Y, Ito N, Yamamoto Y, Owada Y, Kamiya Y, Mitsushima D. 2016. Motor training promotes both synaptic and intrinsic plasticity of layer II/III pyramidal neurons in the primary motor cortex. *Cereb Cortex*. 26:3494–3507.

Kida H, Mitsushima D. 2018. Mechanisms of motor learning mediated by synaptic plasticity in rat primary motor cortex. *Neurosci Res*. 128:14–18.

Kim MS, Koo H, Han SW, Paulus W, Nitsche MA, Kim YH, Yoon JA, Shin YI. 2017. Repeated anodal transcranial direct current stimulation induces neural plasticity-associated gene expression in the rat cortex and hippocampus. *Restor Neurol Neurosci*. 35:137–146.

Kristensen AS, Jenkins MA, Banke TG, Schousboe A, Makino Y, Johnson RC, Huganir R, Traynelis SF. 2011. Mechanism of Ca2+/calmodulin-dependent kinase II regulation of AMPA receptor gating. *Nat Neurosci*. 14:727–735.

Kronberg G, Bridi M, Abel T, Bikson M, Parra LC. 2017. Direct current stimulation modulates LTP and LTD: activity dependence and dendritic effects. *Brain Stimul*. 10:51–58.

Lefaucheur JP. 2016. A comprehensive database of published tDCS clinical trials (2005-2016). *Neurophysiol Clin*. 46:319–398.

Leggio GM, Di Marco R, Gulisano W, D'Ascenzo M, Torrisi SA, Geraci F, Lavanco G, Dahl K, Giurdanella G, Castorina A *et al*. 2019. Dopaminergic-GABAergic interplay and alcohol binge drinking. *Pharmacol Res*. 141:384–391.

Lefebvre S, Liew SL. 2017. Anatomical parameters of tDCS to modulate the motor system after stroke: a review. *Front Neurol*. 8:29.

Lonart G, Wang J, Johnson KM. 1992. Nitric oxide induces neurotransmitter release from hippocampal slices. *Eur J Pharmacol*. 220:271–272.

Lu W, Isozaki K, Roche KW, Nicoll RA. 2010. Synaptic targeting of AMPA receptors is regulated by a CaMKII site in the first intracellular loop of GluA1. *Proc Natl Acad Sci U S A*. 107:22266–22271.

MacDougall MJ, Fine A. 2013. The expression of long-term potentiation: reconciling the preists and the postivists. *Philos Trans R Soc Lond B Biol Sci*. 369:20130135.

Malenka RC, Bear MF. 2004. LTP and LTD: an embarrassment of riches. *Neuron*. 44:5–21.

Márquez-Ruiz J, Leal-Campanario R, Sánchez-Campusano R, Molaee-Ardekani B, Wendling F, Miranda PC, Ruffini G, Gruart A, Delgado-García JM. 2012. Transcranial direct-current stimulation modulates synaptic mechanisms involved in associative learning in behaving rabbits. *Proc Natl Acad Sci U S A*. 109:6710–6715.

McHughen SA, Rodriguez PF, Kleim JA, Kleim ED, Marchal Crespo L, Procaccio V, Cramer SC. 2010. BDNF val66met polymorphism influences motor system function in the human brain. *Cereb Cortex*. 20:1254–1262.

Nitsche MA, Paulus W. 2000. Excitability changes induced in the human motor cortex by weak transcranial direct current stimulation. *J Physiol*. 527:633–639.

Nitsche MA, Fricke K, Henschke U, Schlitterlau A, Liebetanz D, Lang N, Henning S, Tergau F, Paulus W. 2003. Pharmacological modulation of cortical excitability shifts induced by transcranial direct current stimulation in humans. *J Physiol*. 553:293–301.

Nitsche MA, Jaussi W, Liebetanz D, Lang N, Tergau F, Paulus W. 2004. Consolidation of human motor cortical neuroplasticity by D-cycloserine. *Neuropsychopharmacology*. 29:1573–1578.

Nott A, Watson PM, Robinson JD, Crepaldi L, Riccio A. 2008. S-Nitrosylation of histone deacetylase 2 induces chromatin remodelling in neurons. *Nature*. 455:411–415.

Paciello P, Podda MV, Rolesi R, Cocco S, Petrosini L, Troiani D, Fetoni AR, Paludetti G, Grassi C. 2018. Anodal transcranial direct current stimulation affects auditory cortex plasticity in normal-hearing and noise-exposed rats. *Brain Stimul*. 11:1008–1023.

Pelletier SJ, Cicchetti F. 2014. Cellular and molecular mechanisms of action of transcranial direct current stimulation: evidence from in vitro and in vivo models. *Int J Neuropsychopharmacol*. 18:pyu047.

Podda MV, D'Ascenzo M, Leone L, Piacentini R, Azzena GB, Grassi C. 2008. Functional role of cyclic nucleotide-gated channels in rat medial vestibular nucleus neurons. *J Physiol*. 586:803–815.

Podda MV, Cocco S, Mastrodonato A, Fusco S, Leone L, Barbati SA, Colussi C, Ripoli C, Grassi C. 2016. Anodal transcranial direct current stimulation boosts synaptic plasticity and memory in mice via epigenetic regulation of Bdnf expression. *Sci Rep*. 6:22180.

Rahman A, Reato D, Arlotti M, Gasca F, Datta A, Parra LC, Bikson M. 2013. Cellular effects of acute direct current stimulation: somatic and synaptic terminal effects. *J Physiol*. 591:2563–2578.

Rahman A, Lafon B, Parra LC, Bikson M. 2017. Direct current stimulation boosts synaptic gain and cooperativity in vitro. *J Physiol*. 595:3535–3547.

Ranieri F, Podda MV, Riccardi E, Frisullo G, Dileone M, Profice P, Pilato F, Di Lazzaro V, Grassi C. 2012. Modulation of LTP at rat hippocampal CA3-CA1 synapses by direct current stimulation. *J Neurophysiol*. 107:1868–1880.

Rao VL, Butterworth RF. 1996. Kinetics, pharmacology, and autoradiographic distribution of L-[3H] nitroarginine binding sites in rat cerebellum. *J Neurochem*. 66:701–709.

Rebola N, Srikumar BN, Mulle C. 2010. Activity-dependent synaptic plasticity of NMDA receptors. *J Physiol*. 588:93–99.

Reis J, Robertson E, Krakauer JW, Rothwell J, Marshall L, Gerloff C, Wassermann E, Pascual-Leone A, Hummel F, Celnik PA *et al*. 2008. Consensus: "can tDCS and TMS enhance motor learning and memory formation?". *Brain Stimul*. 1:363–369.

Reis J, Schambra HM, Cohen LG, Buch ER, Fritsch B, Zarahn E, Celnik PA, Krakauer JW. 2009. Noninvasive cortical stimulation enhances motor skill acquisition over multiple days through an effect on consolidation. *Proc Natl Acad Sci U S A*. 106:1590–1595.

Rioult-Pedotti MS, Friedman D, Hess G, Donoghue JP. 1998. Strengthening of horizontal cortical connections following skill learning. *Nat Neurosci*. 1:230–234.

Rioult-Pedotti MS, Friedman D, Donoghue JP. 2000. Learning-induced LTP in neocortex. *Science*. 290:533–536.

Rioult-Pedotti MS, Donoghue JP, Dunaevsky A. 2007. Plasticity of the synaptic modification range. *J Neurophysiol*. 98:3688–3695.

Robertson EM, Press DZ, Pascual-Leone A. 2005. Off-line learning and the primary motor cortex. *J Neurosci*. 25:6372–6378.

Rohan JG, Carhuatanta KA, McInturf SM, Miklasevich MK, Jankord R. 2015. Modulating hippocampal plasticity with in vivo brain stimulation. *J Neurosci*. 35:12824–12832.

Roji O, van Kuyck K, Nuttin B, Wenderoth N. 2015. Anodal tDCS over the primary motor cortex facilitates long-term memory formation reflecting use-dependent plasticity. *PLoS One*. 10:e0127270.

Santos AI, Martínez-Ruiz A, Araújo IM. 2015. S-nitrosation and neuronal plasticity. *Br J Pharmacol*. 172:1468–1478.

Sartor GC, Malvezzi AM, Kumar A, Andrade NS, Wiedner HJ, Vilca SJ, Janczura KJ, Bagheri A, Al-Ali H, Powell SK *et al*. 2019. Enhancement of BDNF expression and memory by HDAC inhibition requires BET Bromodomain reader proteins. *J Neurosci*. 39:612–626.

Schulz PE, Cook EP, Johnston D. 1994. Changes in paired-pulse facilitation suggest presynaptic involvement in long-term potentiation. *J Neurosci*. 14:5325–5337.

Selvakumar B, Jenkins MA, Hussain NK, Huganir RL, Traynelis SF, Snyder SH. 2013. S-nitrosylation of AMPA receptor GluA1 regulates phosphorylation, single-channel conductance, and endocytosis. *Proc Natl Acad Sci U S A*. 110: 1077–1082.

Silver RA, Lubke J, Sakmann B, Feldmeyer D. 2003. High-probability uniquantal transmission at excitatory synapses in barrel cortex. *Science*. 302:1981–1984.

Stafford J, Brownlow ML, Qualley A, Jankord R. 2018. AMPA receptor translocation and phosphorylation are induced by transcranial direct current stimulation in rats. *Neurobiol Learn Mem*. 150:36–41.

von Ossowski L, Li LL, Möykkynen T, Coleman SK, Courtney MJ, Keinänen K. 2017. Cysteine 893 is a target of regulatory thiol modifications of GluA1 AMPA receptors. *PLoS One*. 12:e0171489.

Wolters A, Sandbrink F, Schlottmann A, Kunesch E, Stefan K, Cohen LG, Benecke R, Classen J. 2003. A temporally asymmetric Hebbian rule governing plasticity in the human motor cortex. *J Neurophysiol*. 89:2339–2345.

Wu YJ, Lin CC, Yeh CM, Chien ME, Tsao MC, Tseng P, Huang CW, Hsu KS. 2017. Repeated transcranial direct current stimulation improves cognitive dysfunction and synaptic plasticity deficit in the prefrontal cortex of streptozotocin-induced diabetic rats. *Brain Stimul*. 10:1079–1087.

Xu T, Yu X, Perlik AJ, Tobin WF, Zweig JA, Tennant K, Jones T, Zuo Y. 2009. Rapid formation and selective stabilization of synapses for enduring motor memories. *Nature*. 462:915–919.

Yu TH, Wu YJ, Chien ME, Hsu KS. 2018. Transcranial direct current stimulation induces hippocampal metaplasticity mediated by brain-derived neurotrophic factor. *Neuropharmacology*. 144:358–367.

Zimerman M, Heise KF, Hoppe J, Cohen LG, Gerloff C, Hummel FC. 2012. Modulation of training by single-session transcranial direct current stimulation to the intact motor cortex enhances motor skill acquisition of the paretic hand. *Stroke*. 43:2185–2191.